Surface-Enhanced Raman Spectroscopy

Paul L. Stiles, Jon A. Dieringer, Nilam C. Shah, and Richard P. Van Duyne

Department of Chemistry, Northwestern University, Evanston, Illinois 60208; email: vanduyne@chem.northwestern.edu

Annu. Rev. Anal. Chem. 2008. 1:601–26

First published online as a Review in Advance on March 18, 2008

The *Annual Review of Analytical Chemistry* is online at anchem.annualreviews.org

This article's doi: 10.1146/annurev.anchem.1.031207.112814

1936-1327/08/0719-0601$20.00

Key Words

nanoparticles, sensing, plasmonics, electromagnetic enhancement, nanofabrication, vibrational spectroscopy

Abstract

The ability to control the size, shape, and material of a surface has reinvigorated the field of surface-enhanced Raman spectroscopy (SERS). Because excitation of the localized surface plasmon resonance of a nanostructured surface or nanoparticle lies at the heart of SERS, the ability to reliably control the surface characteristics has taken SERS from an interesting surface phenomenon to a rapidly developing analytical tool. This article first explains many fundamental features of SERS and then describes the use of nanosphere lithography for the fabrication of highly reproducible and robust SERS substrates. In particular, we review metal film over nanosphere surfaces as excellent candidates for several experiments that were once impossible with more primitive SERS substrates (e.g., metal island films). The article also describes progress in applying SERS to the detection of chemical warfare agents and several biological molecules.

1. INTRODUCTION

SERS: surface-enhanced Raman spectroscopy

Raman scattering: inelastic scattering of a photon from a molecule in which the frequency change precisely matches the difference in vibrational energy levels

LSPR: localized surface plasmon resonance

It has been 30 years since it was recognized that the Raman spectra of submonolayer coverages of molecules could be acquired on electrochemically roughened coinage metal surfaces (1, 2). Since then, the field of surface-enhanced Raman spectroscopy (SERS) has grown dramatically, demonstrating its power as an analytical tool for the sensitive and selective detection of molecules adsorbed on noble metal nanostructures. Over 5000 research articles, 100 review articles, and several books on SERS have appeared in the literature. Such a large research database provides ample testimony of the impact of SERS on both fundamental and applied studies in fields as diverse as chemistry, physics, materials science, surface science, nanoscience, and the life sciences (3–16).

Understanding the mechanisms of SERS has been a struggle since the early days of its inception, when the primary goal was merely explaining the 10^6-fold intensity enhancement of the normal Raman scattering cross-section. At the time, the enhancement factor, $EF_{SERS} = 10^6$, could be understood as the product of two contributions: (*a*) an electromagnetic enhancement mechanism and (*b*) a chemical enhancement mechanism. These two mechanisms arise because the intensity of Raman scattering is directly proportional to the square of the induced dipole moment, μ_{ind}, which, in turn, is the product of the Raman polarizability, α, and the magnitude of the incident electromagnetic field, E. As a consequence of exciting the localized surface plasmon resonance (LSPR) of a nanostructured or nanoparticle metal surface, the local electromagnetic field is enhanced by a factor of 10, for example. Because Raman scattering approximately scales as E^4, the electromagnetic enhancement factor is of order 10^4. Researchers viewed the chemical enhancement factor of 10^2 as arising from the excitation of adsorbate localized electronic resonances or metal-to-adsorbate charge-transfer resonances (e.g., resonance Raman scattering). It is also worthwhile to note that surface-enhanced resonance Raman scattering with combined SERS and resonance Raman scattering enhancement factors in the 10^9–10^{10} range was possible at the time.

Despite this enhancement, which made SERS orders of magnitude more sensitive than normal Raman spectroscopy, the full power of SERS unfortunately was not utilized until this past decade. Early systems suffered immensely from irreproducibility owing to ill-defined substrates fabricated by electrochemical roughening. Recent advances in nanofabrication and the 1997 discovery of single-molecule SERS (31, 32), the ultimate limit of detection, have caused an explosion of new research and the extension of SERS from an interesting physical phenomenon to a robust and effective analytical technique. In addition, surface preparation and modification techniques (26–28, 77) have also allowed for analyte selectivity. As such, investigators have applied SERS to many analytical systems in recent years, including anthrax detection (29, 77), chemical warfare–stimulant detection (17), in vitro (6, 30, 79) and in vivo (78) glucose sensing, environmental monitoring (18), the monitoring of heterogeneous catalytic reactions (19), and explosive-agent detection (20). The need for new SERS-based sensing, detecting, and monitoring platforms has also driven new instrumental techniques such as the integration of SERS active substrates into fiber-optic assemblies (18).

This review first describes the SERS electromagnetic mechanism (EM) from a practical standpoint, not dwelling on lengthy equations and derivations, by taking a simple spherical model to extract the analytical features of the EM such as wavelength dependence, distance dependence, and overall enhancement factor. Then, we give an overview of modern nanofabrication techniques for SERS active surfaces. Finally, we conclude with examples of the analytical applications of SERS performed by our research group.

Electromagnetic mechanism (EM): theory describing the magnitude of the SERS enhancement factor arising from field enhancement of both the incident and scattered fields

Localized surface plasmon: electromagnetic field–driven coherent oscillation of the surface conduction electrons in a material with negative real and near-zero imaginary dielectric constants

Extinction spectrum: absorption plus elastic scattering spectrum

2. FUNDAMENTALS OF THE SURFACE-ENHANCED RAMAN SPECTROSCOPY ELECTROMAGNETIC MECHANISM

When an electromagnetic wave interacts with a metal surface, the fields at the surface are different than those observed in the far field. If the surface is rough, the wave may excite localized surface plasmons on the surface, resulting in amplification of the electromagnetic fields near the surface. If one assumes that there is enhancement of the intensity of the incident and scattered fields (albeit at different wavelengths), then the possibility of a large enhancement of Raman scattering intensity arises. This notion is commonly known as the EM of SERS and has served as an important model in the understanding of SERS since its discovery in the 1970s (1, 2, 21). Although this mechanism has been the topic of multiple reviews (5, 22–25) and is reasonably well understood, the reinvigorated interest in SERS due to better-defined substrates (26–28), its application to sensing (29, 30), and the observation of single-molecule surface-enhanced resonance Raman scattering (31, 32) has driven a new wave of experiments designed to lay a stronger foundation and provide deeper insight into the EM. These experiments include testing the wavelength dependence of SERS (33, 34) and the distance dependence of SERS (35, 36) and making theoretical calculations to link the small, arbitrarily shaped noble-metal nanoparticle electromagnetic enhancement to observed SERS enhancement factors (37, 38). We begin our treatment of the EM with the origin of electromagnetic enhancement on the nanoscale, the LSPR.

2.1. The Localized Surface Plasmon Resonance

The LSPR occurs when the collective oscillation of valence electrons in a coinage metal nanoparticle is in resonance with the frequency of incident light (**Figure 1**). Understanding features in the characteristic extinction spectrum (absorption plus scattering) can be complex owing to the effects of the dielectric environment, size, and shape on the full width at half-maximum and spectral location. As such, more detailed explanations are available elsewhere, and we concentrate only on features of the LSPR that are directly applicable to the SERS EM (39). Here we consider a quasistatic approach using a spherical nanoparticle of radius a, irradiated by z polarized light of wavelength λ, in the long wavelength limit ($a/\lambda < 0.1$). This leads to the assumption that the electric field around the nanoparticle is uniform (**Figure 1**), which allows Maxwell's equations to be replaced by the Laplace equation of electrostatics (25). Although this approach is useful for predicting the properties of the SERS EM,

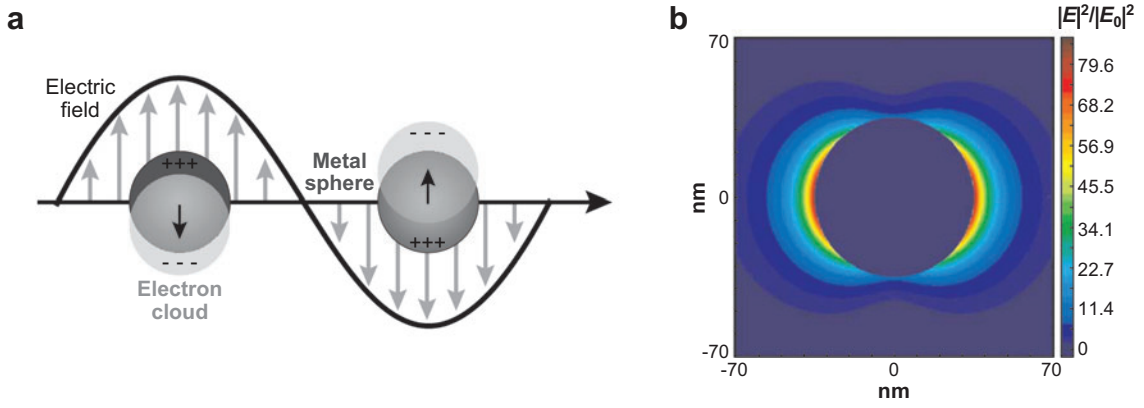

Figure 1

(*a*) Illustration of the localized surface plasmon resonance effect. (*b*) Extinction efficiency (ratio of cross section to effective area) of a spherical silver nanoparticle of 35-nm radius in vacuum $|E|^2$ contours for a wavelength corresponding to the plasmon extinction maximum. Peak $|E|^2 = 85$.

it should not be used as a quantitative treatment as the LSPR extinction of small spherical particles lies in the ultraviolet and is damped by interband transitions and other excitations (12, 40). The resulting analytical solution for the magnitude of the electromagnetic field outside the particle, E_{out}, is given by

$$E_{out}(x, y, z) = E_0\hat{\mathbf{z}} - \alpha E_0\left[\frac{\hat{\mathbf{z}}}{r^3} - \frac{3z}{r^5}\left(x\hat{\mathbf{x}} + y\hat{\mathbf{y}} + z\hat{\mathbf{z}}\right)\right], \quad (1)$$

where x, y, and z are the usual Cartesian coordinates; r is the radial distance; $\hat{\mathbf{x}}$, $\hat{\mathbf{y}}$, and $\hat{\mathbf{z}}$ are the Cartesian unit vectors; and α is the metal polarizability expressed as

$$\alpha = ga^3, \quad (2)$$

where a is the radius of the sphere and g is defined as

$$g = \frac{\varepsilon_{in} - \varepsilon_{out}}{(\varepsilon_{in} + 2\varepsilon_{out})}. \quad (3)$$

Here ε_{in} is the dielectric constant of the metal nanoparticle, and ε_{out} is the dielectric constant of the external environment. The magnitude of the enhancement is wavelength dependent, owing to the strong wavelength dependence of the real portion of the metal nanoparticle dielectric constant. As such, the maximum enhancement occurs when the denominator of g approaches zero ($\varepsilon_{in} \approx -2\varepsilon_{out}$). Examining Equation 1, we also can see that the field enhancement decays with r^{-3}, implying the existence of a finite sensing volume around the nanoparticle. (We discuss these implications in later sections.)

According to Mie theory, the extinction spectrum, $E(\lambda)$, of an arbitrarily shaped nanoparticle is given by

$$E(\lambda) = \frac{24\pi^2 N a^3 \varepsilon_{out}^{3/2}}{\lambda \ln(10)} \left[\frac{\varepsilon_i(\lambda)}{(\varepsilon_r(\lambda) + \chi \varepsilon_{out})^2 + \varepsilon_i(\lambda)^2} \right], \quad (4)$$

where ε_r and ε_i are the real and imaginary components of the metal dielectric function ε_{in}, respectively (41, 42). Again, the real portion of the metal dielectric constant is wavelength dependent. This equation is also generalized from the small sphere solution by replacing the factor of 2 that appears with ε_{out} in Equation 3 with χ, where χ is the shape factor that accounts for deviation from spherical particle geometries into higher aspect ratio structures. This assumption is made because Mie theory cannot be solved analytically for structures other than spheroids. Because χ amplifies ε_{out}, the shape factor is generalized as the sensitivity of the LSPR extinction spectrum to the dielectric environment. The value of χ is 2 for the case of a sphere, but it can take on values as large as 20 (43). The dielectric resonance condition ($\varepsilon_r \approx -\chi \varepsilon_{out}$) is met in the visible region of the spectrum for nanoparticles of high aspect ratio (large χ) comprising coinage metals such as silver and gold. Therefore, it is trivial to perform SERS on pre-existing Raman spectroscopic instrumentation without modification when using these substrates.

Because one can only solve the extinction spectrum analytically for spheres and spheroids, it must be approximated for all other geometries (28, 43). Researchers have developed numerical methods that represent the nanoparticle target with N finite polarizable elements commonly referred to as dipoles. These coupled dipoles interact with the applied field, and by applying the Claussius-Mossotti polarizabilities with some radiative reaction correction (44, 45), one can calculate the extinction and scattering spectra of the target. These methods include the discrete dipole approximation and the finite-difference time domain methods (37, 45, 46), and calculated results typically match well with experiment.

2.2. E^4 Enhancement

In Raman spectroscopy, the scattered intensity is linear with the incident field intensity, E_0^2 (47). Because this field intensity is magnified at the nanoparticle surface, the Raman intensity is therefore related to the absolute square of E_{out} evaluated at the surface of the nanoparticle ($r = a$). Manipulating Equations 1–3, this is given for a small metal sphere by

$$|\mathbf{E}_{\text{out}}|^2 = E_0^2[|1 - g|^2 + 3\cos^2\theta(2\text{Re}(g) + |g|^2)], \quad (5)$$

where θ is the angle between the incident field vector and the vector to the position of the molecule on the surface. The peak enhancement occurs when θ is 0° or 180°, corresponding to the molecule being on the axis of light propagation, and in cases in which g is large, the maximum enhancement approaches $|\mathbf{E}_{\text{out}}|^2 = 4E_0^2|g|^2$. **Figure 2** shows the field intensity as a function of position for a spherical particle. The ratio of

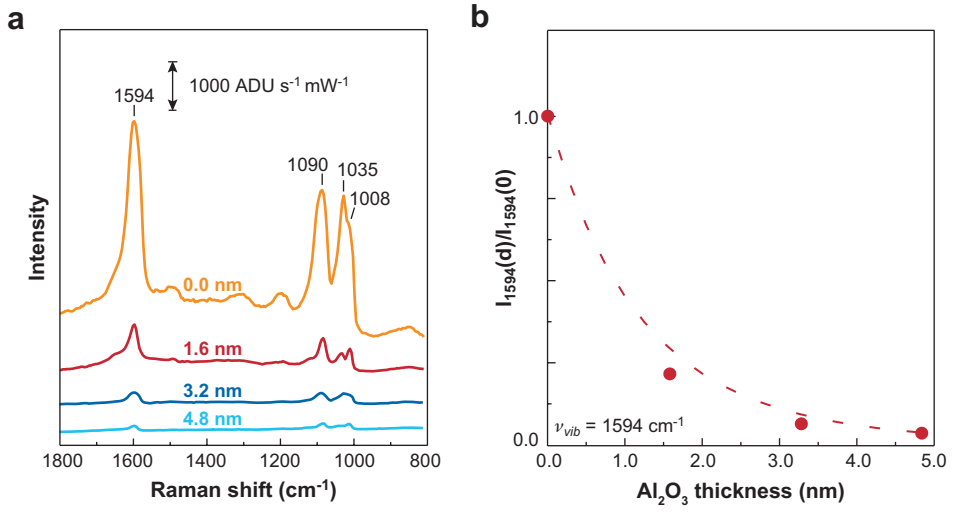

Figure 2

(*a*) Surface-enhanced Raman spectra of pyridine adsorbed to silver film over nanosphere samples treated with various thicknesses of alumina (0.0 nm, 1.6 nm, 3.2 nm, and 4.8 nm). ex = 532 nm, P = 1.0 mW, and acquisition time = 300 s. (*b*) Plot of surface-enhanced Raman spectroscopy intensity as a function of alumina thickness for the 1594 cm^{-1} band (circles). The dashed curved line is a fit of this data to Equation 8 (35). Reproduced with permission from the Royal Society of Chemistry.

the maximum to minimum intensity on a metal sphere is 4, and the radially averaged intensity is $|\overline{\mathbf{E}}_{out}|^2 = 2E_0^2|g|^2$.

In Raman scattering, the applied field induces an oscillating dipole in the molecule on the surface. This dipole then radiates, and there is a small probability that the radiated light is Stokes shifted by the vibrational frequency of the molecule. Although Equation 5 gives a general expression for the enhancement of the incident field, the emission of radiation from the dipole may be enhanced. The treatment for the enhanced emission intensity is more complex and has received proper treatment by Kerker and colleagues (48, 49), but a first-order approximation is to use an expression similar to Equation 5, except evaluated at the Raman Stokes-shifted frequency. Therefore, in this approximation, we can write the following expression:

$$EF = \frac{|\mathbf{E}_{out}|^2|\mathbf{E}'_{out}|^2}{|\mathbf{E}_0|^4} = 4|g|^2|g'|^2, \quad (6)$$

Enhancement factor (EF): magnitude of increase in Raman scattering cross section when the molecule is adsorbed to a SERS-active substrate

where the primed symbols refer to the field evaluated at the scattered frequency. We define this expression as the theoretical SERS EM enhancement factor (EF), and if the Stokes shift is small, both g and g' are at approximately the same wavelength, and the EF scales as g^4. In the literature, this is commonly referred to as E^4 enhancement or the fourth power of field enhancement at the nanoparticle surface. Although this expression was derived using certain approximations, it is identical to that of Kerker's

more rigorous approach. Assuming $|g|$ is approximately 10 for a small sphere in this model, then the magnitude of the SERS EM enhancement is 10^4 to 10^5, and $|g|$ can be much larger in higher-order silver nanostructures in which the EM EFs can approach 10^8 (34).

Although this theoretical treatment of SERS is useful in determining the origin of the often-stated E^4 enhancement approximation, in practical use, it is often simpler to experimentally measure the EF analytically than to predict it theoretically. The EF for a SERS system can be described by

$$EF = \frac{[I_{SERS}/N_{surf}]}{[I_{NRS}/N_{vol}]}, \tag{7}$$

which, evaluated at a single excitation wavelength, describes the average Raman enhancement and accounts for the enhancement of both the incident excitation and the resulting Stokes-shifted Raman fields, where I_{SERS} is the surface-enhanced Raman intensity, N_{surf} is the number of molecules bound to the enhancing metallic substrate, I_{NRS} is the normal Raman intensity, and N_{vol} is the number of molecules in the excitation volume (34, 50). Practically, for a given molecule, one must measure I_{SERS} and I_{NRS} independently and be careful when evaluating spot size and probe volume to determine the EF analytically. McFarland et al. (34) give a detailed approach for measuring SERS EFs.

2.3. Distance Dependence

The SERS distance dependence is critical both mechanistically and practically. The EM predicts that SERS does not require the adsorbate to be in direct contact with the surface but within a certain sensing volume. From a practical perspective, there are certain experiments, such as those involving surface-immobilized biological molecules (51), in which direct contact between the adsorbate of interest and the surface is not possible because the surface is modified with a capture layer for specificity or biocompatibility. Because the field enhancement around a small metal sphere decays with r^{-3}, using the E^4 approximation, the overall distance dependence should scale with r^{-12}. Taking into account the increased surface area scaling with r^2 as one considers shells of molecules at an increased distance from the nanoparticle, one should experimentally observe the r^{-10} distance dependence:

$$I_{SERS} = \left(\frac{a+r}{a}\right)^{-10}, \tag{8}$$

where I_{SERS} is the intensity of the Raman mode, a is the average size of the field-enhancing features on the surface, and r is the distance from the surface to the adsorbate (36).

The ideal distance-dependence experiment is one in which the thickness of the spacer layer could be easily varied in thickness from a few angstroms to tens of nanometers. Furthermore, the spacers would be conformal to handle roughened and nanostructured surfaces, pinhole free, and chemically uniform. Atomic layer

Atomic layer deposition (ALD): self-limiting growth process performed by alternating dosing and saturation of precursors

FON: film over nanosphere

deposition (ALD) is such a spacer fabrication method that produces highly uniform and controlled thin films (52). Precursor gases are alternately pulsed through a reactor and purged away, resulting in a self-limiting growth process that constructs one film layer at a time. A specific number of layers of Al_2O_3 can be deposited with subnanometer-thickness resolution.

We have deposited Al_2O_3 multilayers onto Ag film over nanosphere (AgFON) surfaces to probe the distance dependence of SERS. **Figure 3*a*** shows the SER spectra for pyridine adsorbed on AgFON surfaces coated with four different thicknesses

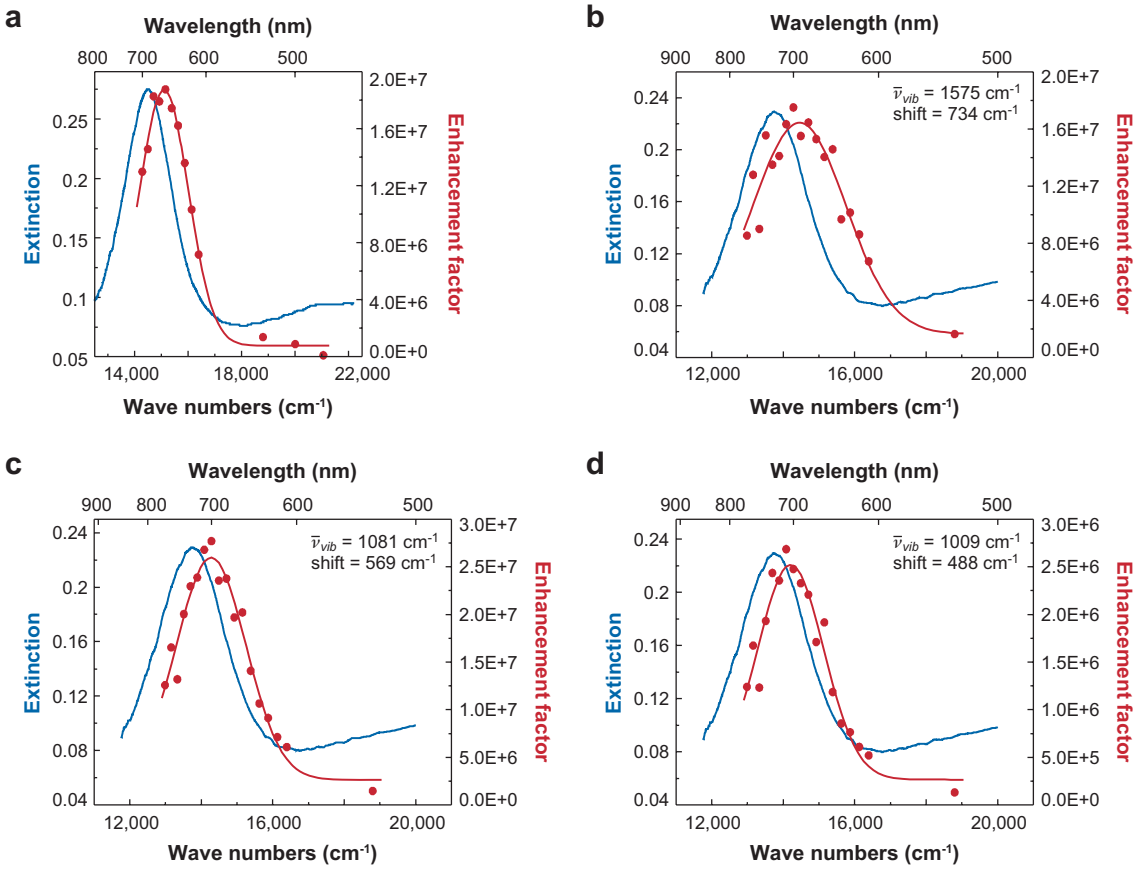

Figure 3

(*a*) Surface-enhanced Raman excitation spectra with Si as intensity standard. Localized surface plasmon resonance (LSPR) $\lambda_{max} = 690$ nm, profile fit maximum at $\lambda_{ex,max} = 662$ nm. (*b–d*) Effect of Stokes Raman shift. (*b*) Profile of the 1575 cm^{-1} vibrational mode of benzenethiol. Distance between LSPR λ_{max} and excitation profile fit line $\lambda_{ex,max} = 734$ cm^{-1}. Enhancement factor (EF) $= 1.8 \times 10^7$. (*c*) 1081 cm^{-1} vibrational mode, shift $= 569$ cm^{-1}, and EF $= 2.8 \times 10^7$. (*d*) 1009 cm^{-1} vibrational mode, shift $= 488$ cm^{-1}, and EF $= 2.7 \times 10^6$. Reproduced with permission from Reference 34. Copyright 2005, American Chemical Society.

of ALD-deposited Al_2O_3. **Figure 3*b*** shows a plot of the relative intensity of the 1594 cm^{-1} band as a function of Al_2O_3 thickness. Fitting the experimental data to Equation 8 leads to the average size of the enhancing particle, $a = 12.0$ nm. The term d_{10} defines the surface-to-molecule distance required to decrease the SERS intensity by a factor of ten. The data presented in this work clearly show that SERS is a long-range effect with a d_{10} value for this particular surface nanostructure of 2.8 nm. This value was derived assuming that a complete monolayer was formed with each ALD cycle. Quartz crystal microbalance measurements have shown that the average thickness of the ALD sequence is 1.1 Å and consequently a complete layer of alumina is not formed with each cycle when repeated layers are formed. The mechanism for the formation of alumina on silver is still debated, but assuming that the quartz crystal microbalance measurements accurately model the first few layers of ALD deposition on silver, the measured value of d_{10} could be as low as 1 nm.

2.4. Surface-Enhanced Raman Spectroscopy Wavelength Dependence

The E^4 enhancement approximation predicts that the best spectral location of the LSPR for maximum EM enhancement is coincident with the laser excitation wavelength. This would lead to maximum enhancement of the incident field intensity at the nanoparticle surface. In practice, this is not the case. According to the theoretical treatment presented in Section 2.2, it is necessary to achieve electromagnetic enhancement of both the incident field and the radiated field, which, for Raman scattering, is at a different wavelength. When the vibrational energy spacing corresponds to the fingerprint region (500–1500 cm^{-1}), the small Stokes-shift approximation breaks down and, consequently, so does the E^4 approximation. Although experiments were proposed at the inception of SERS to measure this effect, studies performed were inconclusive owing to limitations in instrumentation and poor definition of the SERS substrates (53–55). The ideal experiment is to have a continuously tunable excitation and detection scheme over the bandwidth of a well-defined LSPR.

A recently completed systematic study (34) investigated the optimum excitation wavelength as a function of the spectral position of the maximum LSPR extinction. This was made possible by recent advances in nanofabrication and better tunability in both the SERS excitation and detection. **Figure 3*a*** shows a characteristic wavelength scanned excitation profile of the 1081 cm^{-1} peak from benzenethiol. The excitation profile shows the highest SERS EF occurs when the excitation wavelength is higher in energy than the spectral maximum of the LSPR extinction spectrum. A Gaussian fit was made to the profile and distance in energy of the maximum of the excitation profile, and the LSPR extinction spectrum is 613 cm^{-1}, which is on the order of half the vibrational energy, 1081 cm^{-1}. To generalize the magnitude of the profile shift, the experiment was repeated for three vibrational modes in benzenethiol: 1009 cm^{-1}, 1081 cm^{-1}, and 1575 cm^{-1} (**Figure 3*b–d***). As the vibrational energy increases, so does the difference in energy of the maximum of the excitation profile and the maximum of the LSPR extinction spectrum. For all three modes, the magnitude of the separation was approximately half, which agrees with the EM as it predicts that the enhancement of both the incident and scattered fields is important to maximize the SERS EF. The

enhancement of both fields occurs optimally when the frequencies of the incident and scattered fields straddle the LSPR extinction spectrum.

The experiment was also performed on multiple silver nanoparticle sizes and shapes with extinction spectra at various locations in the visible region of the electromagnetic spectrum. The data measured in the experiment are available elsewhere (34), but in all cases, the magnitude of the energy separation between the excitation profile maximum and the LSPR extinction maximum is roughly half. Consequently, to achieve maximum EM enhancement, one should either prepare the sample such that the LSPR extinction is in the proper location for fixed laser frequency apparatuses or set the wavelength to a higher frequency than the LSPR extinction in tunable systems. In the wavelength-scanned experiment, the relevant LSPR extinction spectrum is the one observed after adsorption of the analyte as the LSPR extinction spectrum is sensitive to the dielectric environment. These experiments illustrate the importance of optimizing the plasmon and excitation wavelengths to achieve maximum SERS enhancements.

3. EXPERIMENTAL DETAILS

3.1. Instrumentation

Figure 4 gives a schematic representation of two instrumental approaches to the measurement of SER spectra. The first approach (**Figure 4*a***) is that of the macro-Raman configuration. In this setup, a laser is focused on the SERS substrate at a glancing angle, while the Raman light is collected by a large collection lens. The light is then focused through the entrance slit of a spectrometer and detected using a liquid-nitrogen-cooled charged-coupled device camera. The instrumental approach shown in **Figure 4*a*** is typically used for experiments requiring low spatial resolution and high raw SERS intensity.

For experiments that require higher spatial resolution, the micro-Raman configuration is used (**Figure 4*b***). Laser light is both focused and collected through the same high numerical–aperture objective, after which the scattered light is passed through a notch filter for the removal of Rayleigh-scattered light. Finally the light is focused and directed to a spectrometer and detector. In experiments scanning SER spectra over many different wavelengths, the schematic shown in **Figure 4*c*** is used. This setup employs the use of a series of flipper mirrors for the quick switching between lasers to access nearly the entire visible and near-infrared range of the spectrum.

3.2. Nanofabrication

In the early stages of SERS, most substrates were made using randomly deposited metal films or electrochemically roughened electrodes (5). For example, a thin layer of gold or silver, typically between 5 and 10 nm, was vapor deposited onto a slide, resulting in a collection of thin island films capable of supporting surface plasmons. Although a small amount of tunability is possible through the modification of film

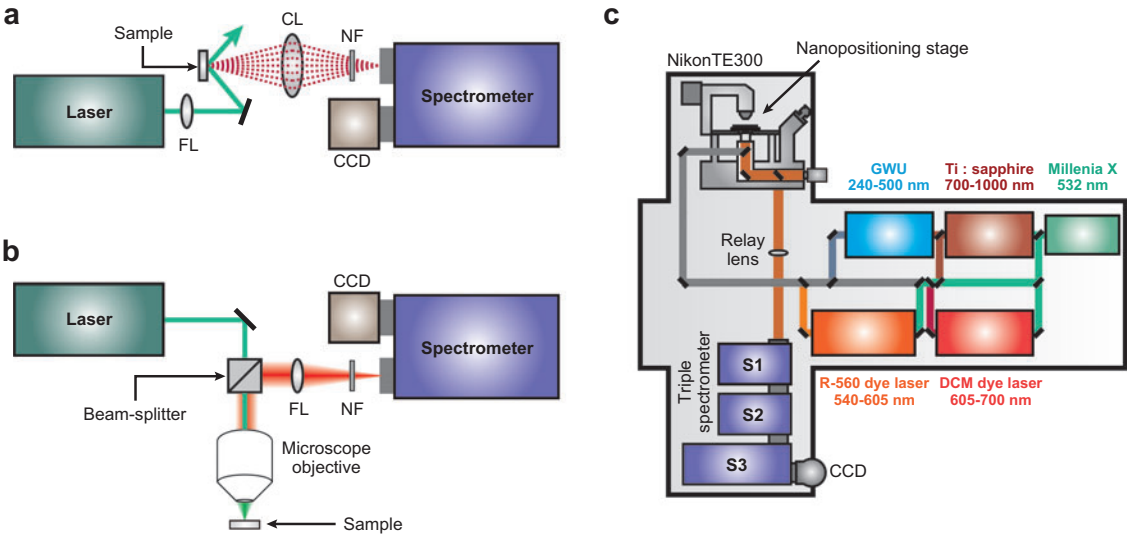

Figure 4

Schematic diagram of typical instrumentation used for surface-enhanced Raman spectroscopy experiments. (*a*) Macro-Raman configuration used when 100-μm-to-millimeter spatial resolution is sufficient. (*b*) Micro-Raman setup, which uses a microscope objective for illumination and collection, increasing the spatial resolution of the instrument. (*c*) Schematic diagram of the experimental setup as laid out on the laser table. The setup allows for easy tunability over the visible wavelengths, using a combination of lasers while maintaining alignment on the sample. The triple spectrograph analyzes Raman scattering excited at wavelengths throughout the visible spectrum. Abbreviations: CCD, charge-coupled device; CL, collection lens; FL, focusing lens; NF, notch filter.

thickness and solvent annealing, variations and a lack of information regarding the SERS active sites prevented a quantitative application of SERS (56, 57).

The past decade has seen significant advances in both the understanding and applications of SERS. One contributing factor in this reinvigoration has been the advances in nanofabrication. The ability to control the shape and orientation of nanoparticles on a surface has reduced many of the complex variables related to SERS and has greatly enhanced our understanding of this phenomenon. A particular nanofabrication method used to great effect in our laboratory is nanosphere lithography (NSL) (58). This method is both cost effective and relatively easy to implement. The process involves drop coating polymer nanospheres on a substrate and then allowing the nanospheres to self-assemble into a close-packed hexagonal array. This array is then used as a mask for the creation of several different SERS active substrates (**Figure 5**). To fabricate periodic nanotriangle arrays, one deposits metal (15–100 nm) directly through the gaps in the nanosphere mask, and upon removal of the mask, a periodic array of nanoscale metal is left. A relatively thick layer of a plasmonic metal (~200 nm) can be deposited directly onto the nanosphere mask. Such metal FON surfaces have an extremely high density of SERS active sites. These FON surfaces are particularly

Nanosphere lithography (NSL): deposition mask formed by self-assembly of hexagonally close-packed nanospheres

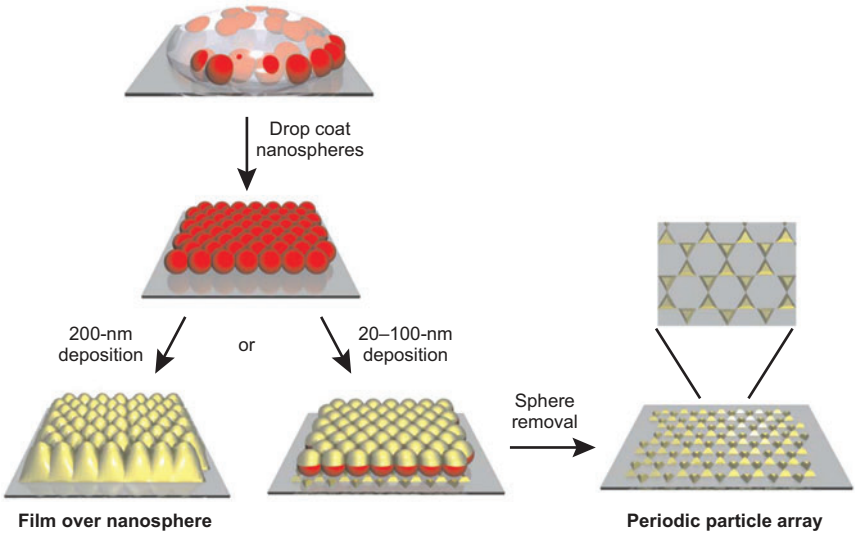

Figure 5

Schematic representation of the nanosphere lithography process for fabricating metal film over nanosphere and periodic particle arrays of metal nanotriangles.

robust and can withstand large environmental perturbations, as discussed below. Finally, the nanosphere layer can be used as an etch mask. Reactive ion etching through the mask creates small wells, into which metal can be deposited (59).

3.3. Optimized Surface-Enhanced Raman Spectroscopy Surfaces

The fundamental requirement for SERS is a substrate that supports a surface plasmon resonance. The search for the optimal SERS substrate is an ongoing endeavor, with many such surfaces being reported in the literature (60–65). A full review of all the current SERS substrates would be impractical, but we briefly mention that nanopatterning techniques have greatly expanded the list of possible surfaces and have uncovered many of the characteristics required for maximum signal enhancement.

With such a large volume of SERS substrates reported, a systematic method for evaluating the surface's SERS characteristics is needed. In essence, the goal is to have the largest amount of SERS active sites combined with the greatest EM EF for each site. To illustrate this simple, but many times forgotten, requirement for SERS surfaces, we compare the EFs and density of SERS active sites on three surfaces.

For a proper comparison to be carried out, we must define an expression that accounts for all the many different variables on a SERS substrate. The following equation contains all the factors that dictate the intensity of a SERS signal:

$$I(\omega_S) = NA\Omega \frac{d\sigma(\omega_S)}{d\Omega} P_L(\omega_L)\varepsilon(\omega_L)^{-1} Q(\omega_S) T_m T_0 EF, \quad (9)$$

where N is the molecule surface density, A is the excitation area, $I(\omega_S)$ is the SERS intensity at Stokes frequency ω_S, Ω is the solid angle of photon collection, $\frac{d\sigma(\omega_S)}{d\Omega}$ is the Raman scattering cross section, $P_L(\omega_L)$ is the radiant flux at excitation frequency, $\varepsilon(\omega_L)$ is the energy of the incident photon, $Q(\omega_S)$ is the quantum efficiency of the detector, T_m is the transmission efficiency of the spectrometer, T_0 is the transmission efficiency of the collection optics, and EF is the enhancement factor.

We can further simplify the above multiplicative expression by conveniently combining several of the known and approximated constants into a single constant, leaving the following:

$$I(\omega_S) = 5.4 \times 10^9 (\mathrm{cm}^{-2} \times \mathrm{torr}^{-1} \times \mathrm{s}^{-2}) \times P_i \times t_{\mathrm{exp}} \times A \times S_i \times a_i \times EF, \quad (10)$$

where it has been assumed that $\Omega = 1$ sr; $\frac{d\sigma(\omega_S)}{d\Omega} = 10^{-30} \frac{\mathrm{cm}^2}{\mathrm{sr} \times \mathrm{molecule}}$; $P_L(\omega_L) = 20$ W cm^{-2}; $Q(\omega_S) = 0.93$; $T_m = 0.75$; $T_0 = 0.86$; and finally a sticking probability (S_i), an estimate of fraction of SERS active sites (a_i), and exposure time (t_{exp}) at partial pressure (P_i) have been added to approximate the number of molecules in the probe area (A).

With a simple expression that includes all the relevant factors that dictate SERS intensity, it is now possible to compare the theoretical limits of detection for SERS active surfaces. In the case of the AgFON, the EF has been measured to be 10^7 (66), whereas the fraction of molecules residing in SERS active sites is essentially unity. Using Equation 9, assuming a 1-s exposure time and an illuminated area of 10^{-4} cm^2, the calculated SERS intensity is 4×10^5 counts s^{-1} ppb^{-1}. With regard to the triangular nanoparticle array fabricated with NSL (**Figure 5**), larger EFs have been reported and are typically on the order of 10^8 (25). Contrary to the FON, there are much fewer active sites on the NSL fabricated surface, and if the fraction of molecules residing on SERS active sites within the illuminated area is assumed to be 0.07, then the SERS intensity is calculated to be 3×10^5 counts s^{-1} ppb^{-1}, slightly smaller than the AgFON surface. To further illustrate the importance of EFs as well as SERS active sites, we examine the theoretical SERS intensity of a substrate drop coated with colloidal silver aggregate. These randomly prepared aggregates provide extremely large EFs of 10^{14} and have been found to be responsible for single-molecule SERS (31, 32). Given that the SERS enhancement relies on the uncontrolled orientation of the silver colloids and the random binding of the analyte molecules to one of the SERS hot spots, the fraction of molecules within the illuminated area is quite small. If the estimated fraction is 10^{-10}, the SERS intensity turns out to be 4×10^2 counts s^{-1} ppb^{-1}, much less than either the FON or NSL fabricated triangle array. The above comparison illustrates the importance of including the density of SERS active sites on a substrate as well as the EF when considering the optimal substrate for a given application.

4. FUNCTIONALIZED SURFACES AND APPLICATIONS

4.1. Surface-Enhanced Raman Spectroscopy Sensing

SERS has great potential for chemical and biological sensing applications because it is selective and sensitive and gives little interference from water. Owing to the

SAM: self-assembled monolayer

distance dependence of SERS, an important criterion for these sensors is that the analyte of interest must be within a few nanometers of the nanostructured surface. This can be achieved by either drop coating the analyte directly on bare-metal FONs or using various surface functionalization techniques to bring the analyte closer to the noble-metal structure.

Although some substances can be detected on bare FONs, these substrates are not stable owing to oxidation of the metal surface (67, 68). In addition, some important analytes, such as glucose, have low affinity toward the bare metal surface. Furthermore, bare FON substrates do not have any mechanism for isolating the compound of interest from interferents. To overcome these limitations, investigators have used several methods to functionalize SERS substrates. SERS detection is usually facilitated by the use of various coatings ranging from simple alkanethiolates to complex macrocyclic molecules (69). These molecules are anchored to the noble-metal surface by a thiolate group and form self-assembled monolayers (SAMs). The SAM can separate the analyte of interest from interfering analytes and bring it closer to the nanostructured surface, analogous to the use of a stationary phase in high-performance liquid chromatography. Although SAMs have been useful for many applications, thermal desorption (70, 71) and photooxidation (72–74) can result in defects in the coatings and thermodynamically unstable substrates (75).

ALD offers an alternative technique for forming functionalized SERS substrates that can overcome many of the limitations of SAMs (35). Highly controlled thin films are produced by a self-limiting growth process. ALD broadens the scope of SERS sensors by offering new functionalities to the SERS substrates. One such substrate is alumina-functionalized AgFON substrates. Alumina is commonly used as a stationary phase in chromatography and has a predictable affinity based on polarity. Quartz crystal microbalance measurements have demonstrated a uniform growth rate of ~1 Å per deposition cycle (52). Because the SERS signal is highly distance dependent, this subnanometer thickness is highly advantageous for preserving the sensitivity of SERS. In addition, alumina is extremely stable against oxidation and high temperatures and can significantly increase the lifetime of SERS substrates (76, 77). Research is also underway to coat substrates with other ALD materials, such as titania, introducing even more functionalities for SERS sensing.

An example of a SERS-based sensor functionalized with a SAM is the in vivo glucose sensor. AgFON substrates are modified with a mixed SAM consisting of decanethiol (DT) and mercaptohexanol (MH) (30). DT/MH has dual hydrophobic and hydrophilic properties, making it ideal for in vivo glucose detection. To successfully monitor glucose fluctuations throughout the day, an in vivo glucose sensor must be reversible and stable, have a quick temporal response, and be able to detect physiologically relevant glucose concentrations accurately. We demonstrated the reversibility of the DT/MH AgFON sensor by alternatively exposing the sensor to 0- and 100-mM aqueous glucose solutions (pH ~ 7) (30). **Figure 6*a*** shows the SERS spectra of a DT/MH-functionalized AgFON in phosphate-buffered saline. **Figure 6*b*,*c*** shows the difference spectra demonstrating reversible partitioning and departitioning. In addition, we demonstrated 10-day stability and a temporal response of <30 s (30). Quantitative detection has also been demonstrated in vitro as well as in vivo using

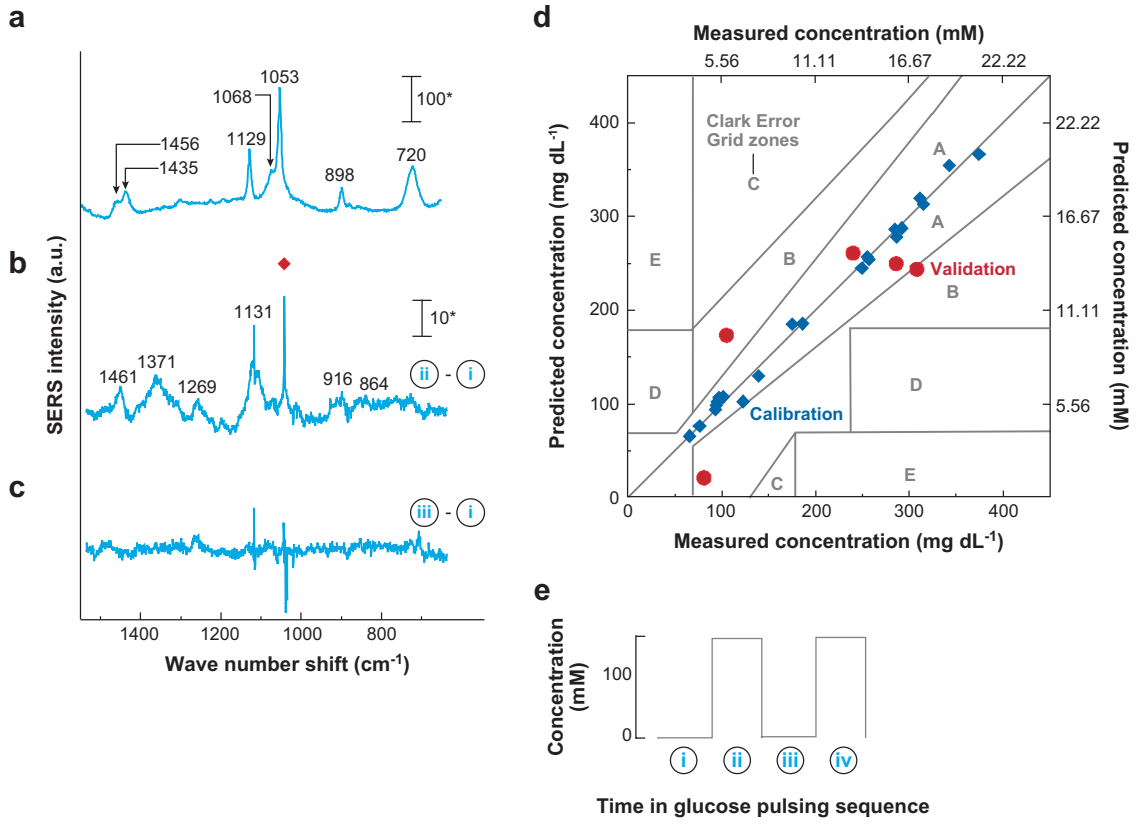

Figure 6

Glucose reversibility and partial least-squares leave-one-out analysis. Glucose pulsing sequence on the self-assembled monolayer–modified Ag film over nanosphere (AgFON) surface for reversibility experiments. (*a*) Surface-enhanced Raman spectra of the decanethiol/mercaptohexanal (DT/MH)-functionalized AgFON in 0-mM phosphate buffered saline solution. $\lambda_{ex} = 532$ nm, $P_{laser} = 10$ mW, $t = 20$ min, and pH ~ 7. (*b*) Difference spectra showing partitioning of glucose. (*c*) Difference spectra showing departitioning of glucose. The red diamond marks the imperfect subtraction of the narrow band at 1053 cm^{-1} due to nitrate, resulting in a sharp peak in the difference spectra. Asterisks denote analog-to-digital units (mW^{-1} min^{-1}). (*d*) Calibration (*blue diamonds*) and validation (*red circles*) plot using a single substrate and a single spot on a DT/MH-functionalized AgFON. Calibration plot was constructed using 21 data points, and validation plot was constructed using five data points taken over a range of glucose concentrations (10–450 mg dl^{-1}) in vivo (rat). RMSEC = 7.46 mg dl^{-1} (0.41 mM) and RMSEP = 53.42 mg dl^{-1} (2.97 mM) with four loading vectors. $\lambda_{ex} = 785$ nm, $P_{laser} = 50$ mW, and $t = 2$ min. Figure reproduced with permission from Reference 78. Copyright 2006, American Chemical Society.

partial least-squares chemometric analysis (30, 78). **Figure *6d*** depicts the in vivo calibration and validation models of a DT/MH-functionalized AgFON substrate implanted in a rat. Finally, we have extended the scope of the DT/MH-functionalized AgFON sensor for multi-analyte detection. The experiment was conducted by

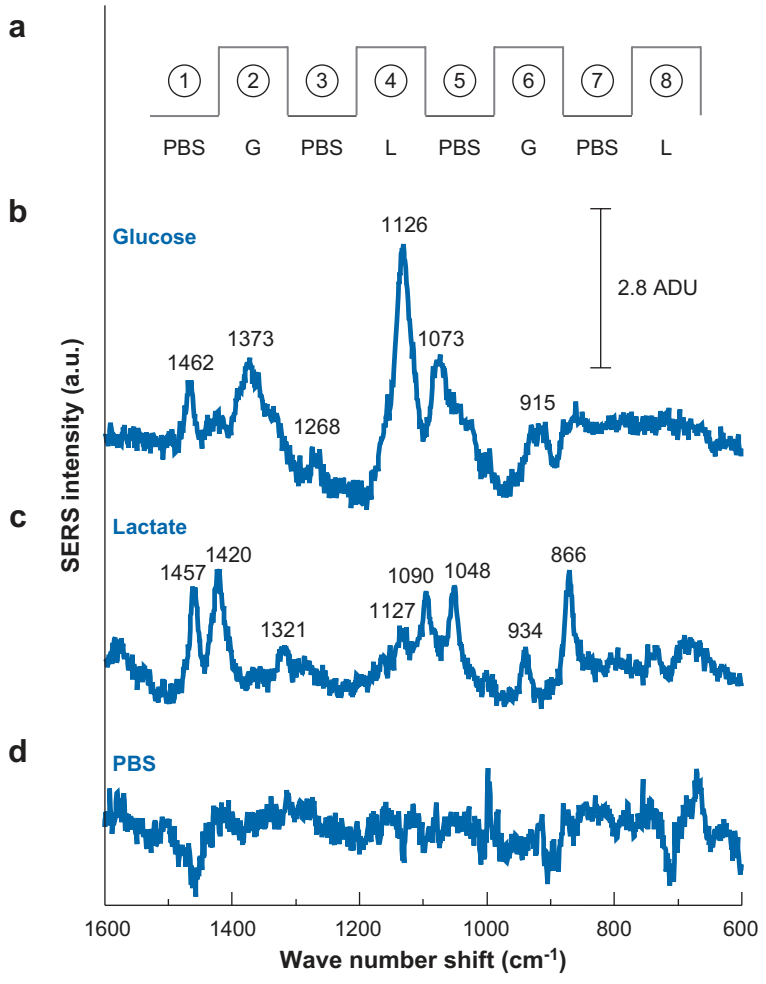

Figure 7

Sequential glucose and lactate pulsing. (*a*) Step changes of glucose (G) and lactate (L) concentrations (0–100 mM) introduced into the sensor. (*b*) Mean difference spectrum (average of difference between steps 2 and 1, and 6 and 5) demonstrating partitioning of glucose. (*c*) Mean difference spectrum (average of difference between steps 4 and 3, and 8 and 7) demonstrating partitioning of lactate. (*d*) Representative difference spectrum of consecutive rinsing steps (3 and 1) demonstrating departitioning of glucose. PBS, phosphate buffered saline; a.d.u., analog-to-digital units. $\lambda_{ex} = 532$ nm, $P = 13$ mW, and $t_{acq} = 10$ min. Figure reproduced with permission from Reference 79. Copyright 2007, American Chemical Society.

alternately injecting 100-mM glucose and 100-mM lactate solutions into the flow cell and rinsing the surface with phosphate-buffered saline between each step. The results indicate that both analytes partition and departition successfully from the DT/MH-functionalized SAM (**Figure 7**) (79).

A SERS-based sensor using alumina-functionalized AgFON substrates has also been fabricated to quantitatively detect an anthrax biomarker, calcium dipicolinate (CaDPA). In this case, CaDPA was initially sensed on bare AgFON substrates and then optimized using alumina. CaDPA (a carboxylic acid) was extracted from *Bacillus subtilis*, a harmless analog of *B. anthracis*, by sonicating in dilute nitric acid and drop coating on bare AgFON substrates. The average intensity of the 1020 cm^{-1} peak was used to construct the adsorption isotherm and determine the limit of detection of CaDPA. Researchers found a limit of detection of 2600 spores and a temporal stability of 3–10 days for the bare AgFON substrates (29). The use of an alumina capture layer produced by ALD significantly increased the sensitivity and stability of the anthrax sensor. Alumina imparts a new functionality to AgFON substrates because of its high affinity for carboxylic acids. Researchers have demonstrated that two cycles of alumina increase the limit of detection to1400 spores (77). The alumina layer also improves the temporal stability of the substrate to at least 9 months by preventing oxidation of the AgFON surface (77).

4.2. Transition-Metal Surface-Enhanced Raman Spectroscopy

Although investigators have demonstrated SERS using several different transition metals (80–82), the vast majority of work has relied on the coinage metals: Cu, Ag, and Au. Such metals support plasmons in the visible region and are resistant to corrosion. Although resistance to degradation might be a desirable characteristic in the simple identification of molecular adsorbates to the surface, it is a definite drawback when trying to apply SERS to the monitoring of heterogeneous catalytic processes.

In an effort to apply SERS to more diverse systems and to possibly use the technique to track a catalytic reaction, several groups have turned to thin overlayers of various transition metals on top of plasmonic metal surfaces or nanoparticles (9, 82, 83). The idea is to retain the surface plasmon of the coinage metal while changing the reactivity of the surface. This technique has been dubbed borrowed SERS, as the catalytically active metal film is thin enough to borrow the EM enhancement of the underlying plasmonic metal. The technique faces many challenges. For one, to avoid the dampening of the plasmon of the underlying metal, one must ensure that the catalytically active overlayer is sufficiently thin. Conversely, the layer must be thick enough to ensure full coverage and minimize any pinholes. Such pinhole-free overlayers will minimize any SERS signal arising from the analyte binding directly to the SERS active metal, instead of the catalytically active metal. Recently, reports on SERS using pure transition metals, such as palladium and platinum, have appeared in the literature (9, 80, 82). These surfaces generally have relatively weak EFs, on the order of 1000, and owe much of that enhancement to the lightning-rod effect (80). With the application of many recent nanofabrication techniques, a refinement in the understanding of transition-metal SERS and borrowed SERS is likely to arise.

4.3. Metal Film over Nanosphere: Universal Surface-Enhanced Raman Spectroscopy Substrate

As it is now well known, the EF of a particular SERS active surface results primarily from the nanostructures on it. A SERS substrate must possess the structures necessary

to support either SPRs or LSPRs. Although it is now possible to engineer surfaces of many different structures, many early SERS substrates (vapor-deposited metal island films and electrochemically roughened surfaces) were plagued with irreproducible EFs. The most common limitation of these early substrates was the so-called irreversible loss phenomenon. Specifically, the nanostructures on the surfaces were only metastable, and once a large-enough perturbation was applied to the surface, the nanostructuring was lost, along with the SERS activity. As a result, SERS has been systematically ignored as a detection solution for many applications.

In our laboratory we have demonstrated that, with the proper substrate, SERS can indeed be used in many applications that were once thought impossible. One example application is the coupling of SERS to temperature-programmed desorption in ultrahigh-vacuum environments (84). It was once thought that SERS would be practically useless for a temperature-programmed-desorption substrate because once the temperature was ramped to high-enough levels, the nanostructures would anneal and SERS activity would be irreversibly lost. However, a relatively recent publication demonstrated that an Ag film deposited over silica nanospheres (AgFON) could be used to create high EF SERS substrates (see **Figure 5**) that were ultrahigh-vacuum compatible. These AgFON surfaces were reproducible, stable, and predictable over large temperature ranges. For a demonstration of the utility of AgFON surfaces in ultrahigh-vacuum, temperature-programmed-desorption studies, benzene, pyridine, and C_{60} were deposited and then thermally desorbed for several cycles while monitoring their SERS intensity. **Figure 8** presents the SERS intensity of the 992 cm^{-1} band of benzene as a representative spectrum. As seen in **Figure 8*a***, after an initial

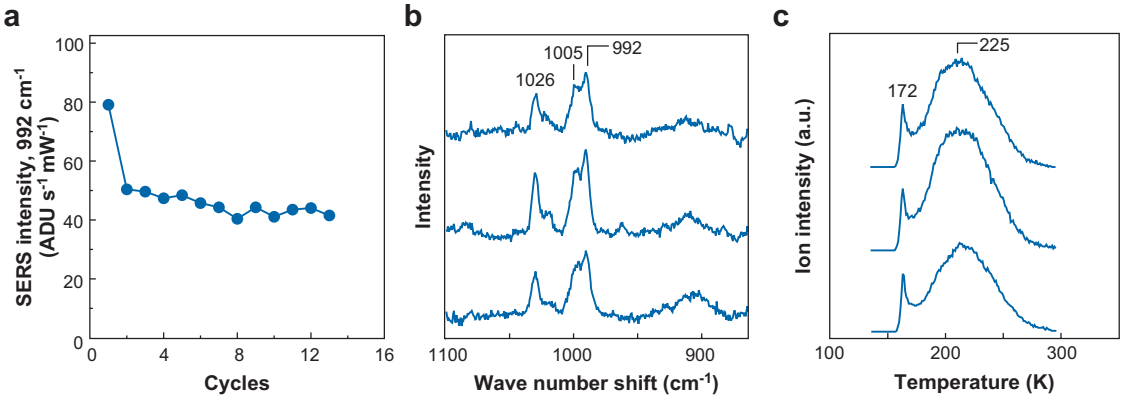

Figure 8

Stability of Ag film over nanosphere (AgFON) toward replicate adsorption-desorption cycles of benzene and pyridine. (*a*) Surface-enhanced Raman spectroscopy (SERS) intensity of the 992 cm^{-1} peak of benzene. Each cycle consists of adsorption of benzene at $T_{surf} = 110$ K and thermal desorption at 300 K with $\beta = 4\ Ks^{-1}$. SERS spectra were taken with 18 mW of $\lambda_{ex} = 514.5$ nm for 60 s. (*b*) Replicate SERS spectra in the 900–1100 cm^{-1} region of pyridine on the AgFON surface collected using 8 mW of $\lambda_{ex} = 632.8$ nm for 60 s. (*c*) The corresponding temperature-programmed-desorption spectra of pyridine desorbing from the AgFON at $\beta = 4\ Ks^{-1}$.

decline, the SERS intensity remains virtually constant over 13 cycles ranging from 110 K to 300 K. **Figure 8*b*** shows the corresponding SER spectra after a typical cycle. The experiments clearly demonstrate the possibility of using AgFON-based SERS substrates in experiments requiring large temperature ranges, as the surface displayed both temporal stability and reproducibility.

The AgFON was not only resistant to large temperature perturbations (as discussed above), but it resisted electrochemical perturbations as well (26, 51, 85). Using typical electrochemically roughened SERS electrodes for electrochemically based SERS experiments has proven to be difficult, due mainly to irreproducibility problems and an irreversible loss of the SERS activity of the surface as potentials and electrolyte concentrations reach extreme levels. Similar to the large temperature changes discussed above, these large potential and electrolyte changes presumably perturb the metastable nanostructure of the SERS electrode, causing an irreversible loss of the nanostructures that support the surface plasmons. As a result, most electrochemical SERS experiments, using traditional metal oxidation-reduction cycle (MORC) roughened electrodes, were limited to relatively modest potential ranges. SERS electrodes based on the metal FON do not show the same signal losses at large potentials measured using MORC electrodes (26). **Figure 9** shows a representation of the difference between the metal FON and the MORC-based electrodes. The AgFON surface (**Figure 9*a***) clearly shows that SERS intensity is retained as the potential ranges from extremely negative (–1200 mV) back to more positive, whereas the AgORC-based electrode has its SERS intensity decrease dramatically at negative potentials, never to return.

With the difficulties using MORC and metal island films as SERS substrates, it might be tempting to turn to metal colloids as an alternative. This would allow the investigation of many biomolecular systems that denature on bare Ag or Au surfaces (86, 87). Although metal colloids support surface plasmons and therefore should be viable SERS substrates, they still have many difficulties with regard to reproducibility and stability to changing environmental conditions. For example, when using silver or gold colloids, changes in the solution ionic strength, pH, electrolyte, composition, and target molecule concentration can cause uncontrollable aggregation of the colloid. Again, owing to its stability over wide temperature, potential, and concentration ranges, the AgFON can be used for the SERS investigation of many biologically important molecules. Given the tendency of large biomolecules to denature over bare Ag or Au surfaces, the functionalization of the AgFON surface with an alkanethiol-based SAM is often required. The SAM effectively separates the bare metal from the biomolecule of interest, thus preventing its breakdown. This method has been demonstrated recently by functionalizing an AgFON with carboxylic acid–terminated alkanethiolates and investigating the distance and orientation dependence of electron transfer in cytochrome *c* (51). The important practical significance of the work demonstrated the possibility of SERS spectroelectrochemistry experiments over a wide range of ionic strength, pH, electrolyte, and redox potentials. The stability of the functionalized AgFON enables the SERS studies of adsorbed biomolecules as a function of these important biophysical variables, which have not been previously accessible.

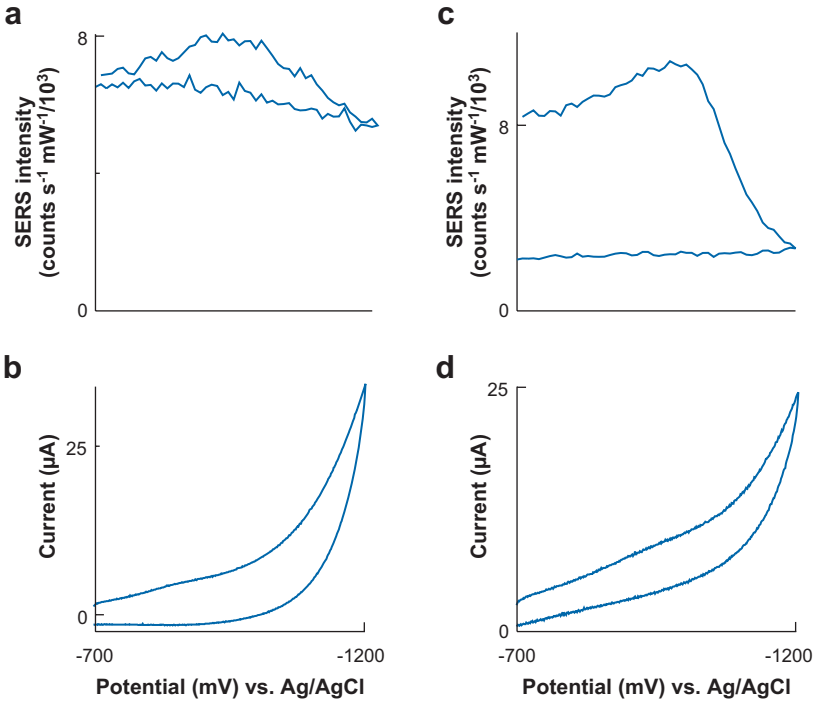

Figure 9

Surface-enhanced Raman spectroscopy (SERS) detected cyclic voltammograms. SERS intensity of the 1008 cm^{-1} band of pyridine (ring breathing mode) versus potential. (*a*) Ag film over nanosphere (AgFON) electrode and (*c*) in situ Ag oxidation-reduction cycle (AgORC) electrode (25 mC cm^{-2}). Laser excitation was 632.8 nm at 4 mW, 0.1-s dwell time, 50-mM pyridine in 0.1-mM KCl. The onset of H_2 evolution from (*b*) AgFON and (*d*) AgORC electrodes is indicated by the increase in current between –1.1 and –1.2 V.

The development of these AgFON-based SERS experiments is important for one practical reason: They demonstrate that the irreversible loss phenomenon, previously thought to be universal to all SERS active substrates, is in fact particular to the SERS substrate under investigation. The primary cause for the irreducible loss of SERS activity of metal island films and MORC-type surfaces can be traced to the alteration of the metastable nanostructures responsible for the surface plasmons. The AgFON SERS substrate, conversely, is reproducible, stable, cost effective, and robust enough to remain SERS active over large temperature, potential, and concentration ranges. Given these results, we believe that many of the applications thought to be impractical for SERS-based detection can now be considered.

DISCLOSURE STATEMENT

The authors receive research funding under the following grants: NSF grants DMR-0520513, EEC-0647560, CHE-0414554, and BES-0507036; AFOSR/MURI grant

F49620-02-1-0381; DTRA JSTO Program (grant FA9550-06-1-0558); DOE grant DE-FG02-03ER15457; NIH grant 4 R33 DK066990-02; and grant U54CA119341 from the NIH National Cancer Institute.

ACKNOWLEDGMENTS

The authors gratefully acknowledge Professor George C. Schatz for his assistance with theoretical calculations and many helpful discussions. This work was supported by NSF grants DMR-0520513, EEC-0647560, CHE-0414554, and BES-0507036; AFOSR/MURI grant F49620-02-1-0381; DTRA JSTO Program (Grant FA9550-06-1-0558); DOE grant DE-FG02-03ER15457; NIH grant 4 R33 DK066990-02; and grant number U54CA119341 from the NIH National Cancer Institute. The contents of the review are solely the responsibility of the authors and do not necessarily represent the official views of the NSF, AFOSR, DOE, or the NIH.

LITERATURE CITED

1. Jeanmarie DL, Van Duyne RP. 1977. Surface Raman spectroelectrochemistry, part 1: heterocyclic, aromatic, and aliphatic amines adsorbed on the anodized silver electrode. *J. Electroanal. Chem.* 84:120
2. Albrecht MG, Creighton JA. 1977. Anomalously intense Raman spectra of pyridine at a silver electrode. *J. Am. Chem. Soc.* 99:5215–17
3. Campion A, Kambhampati P. 1998. Surface-enhanced Raman scattering. *Chem. Soc. Rev.* 27:241–50
4. Kneipp K, Kneipp H, Itzkan I, Dasari RR, Feld MS. 1999. Surface-enhanced Raman scattering: a new tool for biomedical spectroscopy. *Curr. Sci.* 77:915–24
5. Moskovits M. 1985. Surface-enhanced spectroscopy. *Rev. Mod. Phys.* 57:783–826
6. Stuart DA, Yonzon CR, Zhang XY, Lyandres O, Shah NC, et al. 2005. Glucose sensing using near-infrared surface-enhanced Raman spectroscopy: gold surfaces, 10-day stability, and improved accuracy. *Anal. Chem.* 77:4013–19
7. Braun G, Lee SJ, Dante M, Nguyen TQ, Moskovits M, Reich N. 2007. Surface-enhanced Raman spectroscopy for DNA detection by nanoparticle assembly onto smooth metal films. *J. Am. Chem. Soc.* 129:6378–79
8. Braun G, Pavel I, Morrill AR, Seferos DS, Bazan GC, et al. 2007. Chemically patterned microspheres for controlled nanoparticle assembly in the construction of SERS hot spots. *J. Am. Chem. Soc.* 129:7760–61
9. Ren B, Liu GK, Lian XB, Yang ZL, Tian ZQ. 2007. Raman spectroscopy on transition metals. *Anal. Bioanal. Chem.* 388:29–45
10. Chen LC, Ueda T, Sagisaka M, Hori H, Hiraoka K. 2007. Visible laser desorption/ionization mass spectrometry using gold nanorods. *J. Phys. Chem. C* 111:2409–15
11. Willets KA, Van Duyne RP. 2007. Localized surface plasmon resonance spectroscopy and sensing. *Annu. Rev. Phys. Chem.* 58:267–97
12. Schatz GC, Young MA, Van Duyne RP. 2006. Electromagnetic mechanism of SERS. See Ref. 88, pp. 19–45

13. Kneipp K, Kneipp H, Bohr HG. 2006. Single-molecule SERS spectroscopy. See Ref. 88, pp. 261–77
14. Kneipp J. 2006. Nanosensors based on SERS for applications in living cells. See Ref. 88, pp. 335–49
15. Yonzon CR, Lyandres O, Shah NC, Dieringer JA, Van Duyne RP. 2006. Glucose sensing with surface-enhanced Raman spectroscopy. See Ref. 88, pp. 367–79
16. Vo-Dinh T, Yan F, Wabuyele MB. 2006. Surface-enhanced Raman scattering for biomedical diagnostics and molecular imaging. See Ref. 88, pp. 409–26
17. Stuart DA, Biggs KB, Van Duyne RP. 2006. Surface-enhanced Raman spectroscopy of half-mustard agent. *Analyst* 131:568–72
18. Stokes DL, Alarie JP, Ananthanarayanan V, Vo-Dinh T. 1999. Fiber optic SERS sensor for environmental monitoring. *Proc. SPIE.* 3534:647–54
19. Kundu S, Mandal M, Ghosh SK, Pal T. 2004. Photochemical deposition of SERS active silver nanoparticles on silica gel and their application as catalysts for the reduction of aromatic nitro compounds. *Journal of Colloid and Interface Science*. 272:134–44
20. Sylvia JM, Janni JA, Klein JD, Spencer KM. 2000. Surface-enhanced Raman detection of 2,4-dinitrotoluene impurity vapor as a marker to locate landmines. *Anal. Chem.* 72:5834–40
21. Fleischmann M, Hendra PJ, McQuillan AJ. 1974. Raman spectra of pyridine adsorbed at a silver electrode. *Chem. Phys. Lett.* 26:163–66
22. Kerker M. 1984. Electromagnetic model for surface-enhanced Raman-scattering (SERS) on metal colloids. *Acc. Chem. Res.* 17:271–77
23. Metiu H, Das P. 1984. The electromagnetic theory of surface enhanced spectroscopy. *Annu. Rev. Phys. Chem.* 35:507–36
24. Moskovits M. 2005. Surface-enhanced Raman spectroscopy: a brief retrospective. *J. Raman Spectrosc.* 36:485–96
25. Schatz GC, Van Duyne RP. 2002. Electromagnetic mechanism of surface-enhanced spectroscopy. In *Handbook of Vibrational Spectroscopy*, ed. JM Chalmers, PR Griffiths, pp. 759–74. New York: Wiley
26. Dick LA, McFarland AD, Haynes CL, Van Duyne RP. 2002. Metal film over nanosphere (MFON) electrodes for surface-enhanced Raman spectroscopy (SERS): improvements in surface nanostructure stability and suppression of irreversible loss. *J. Phys. Chem. B* 106:853–60
27. Jensen TR, Malinsky MD, Haynes CL, Van Duyne RP. 2000. Nanosphere lithography: tunable localized surface plasmon resonance spectra of silver nanoparticles. *J. Phys. Chem. B* 104:10549–56
28. Malinsky MD, Kelly KL, Schatz GC, Van Duyne RP. 2001. Nanosphere lithography: effect of substrate on the localized surface plasmon resonance spectrum of silver nanoparticles. *J. Phys. Chem. B* 105:2343–50
29. Zhang X, Young MA, Lyandres O, Van Duyne RP. 2005. Rapid detection of an anthrax biomarker by surface-enhanced Raman spectroscopy. *J. Am. Chem. Soc.* 127:4484–89
30. Lyandres O, Shah NC, Yonzon CR, Walsh JT, Glucksberg MR, Van Duyne RP. 2005. Real-time glucose sensing by surface-enhanced Raman spectroscopy

in bovine plasma facilitated by a mixed decanethiol/mercaptohexanol partition layer. *Anal. Chem.* 77:6134–39
31. Nie SM, Emery SR. 1997. Probing single molecules and single nanoparticles by surface-enhanced Raman scattering. *Science* 275:1102–6
32. Kneipp K, Wang Y, Kneipp H, Perelman LT, Itzkan I, et al. 1997. Single molecule detection using surface-enhanced Raman scattering (SERS). *Phys. Rev. Lett.* 78:1667–70
33. Haynes CL, Van Duyne RP. 2003. Plasmon-sampled surface-enhanced Raman excitation spectroscopy. *J. Phys. Chem. B* 107:7426–33
34. McFarland AD, Young MA, Dieringer JA, Van Duyne RP. 2005. Wavelength-scanned surface-enhanced Raman excitation spectroscopy. *J. Phys. Chem. B* 109:11279–85
35. Dieringer JA, McFarland AD, Shah NC, Stuart DA, Whitney AV, et al. 2005. Surface enhanced Raman spectroscopy: new materials, concepts, characterization tools, and applications. *Faraday Discuss.* 132:9–26
36. Kennedy BJ, Spaeth S, Dickey M, Carron KT. 1999. Determination of the distance dependence and experimental effects for modified SERS substrates based on self-assembled monolayers formed using alkanethiols. *J. Phys. Chem. B* 103:3640–46
37. Yang W-H, Schatz GC, Van Duyne RP. 1995. Discrete dipole approximation for calculating extinction and Raman intensities for small particles with arbitrary shapes. *J. Chem. Phys.* 103:869–75
38. Zeman EJ, Schatz GC. 1987. An accurate electromagnetic theory study of surface enhancement factors for silver, gold, copper, lithium, sodium, aluminum, gallium, indium, zinc, and cadmium. *J. Phys. Chem.* 91:634–43
39. Kelly KL, Coronado E, Zhao L, Schatz GC. 2003. The optical properties of metal nanoparticles: the influence of size, shape, and dielectric environment. *J. Phys. Chem. B* 107:668–77
40. Kreibig U, Vollmer M. 1995. *Optical Properties of Metal Clusters*. Berlin: Springer
41. Bohren CR, Huffman DF. 1983. *Absorption and Scattering of Light by Small Particles*. New York: Wiley
42. Mie G. 1908. Contributions to the optics of turbid media, especially colloidal metal solutions. *Ann. Phys.* 25:377–445
43. Link S, El-Sayed MA. 1999. Spectral properties and relaxation dynamics of surface plasmon electronic oscillations in gold and silver nano-dots and nano-rods. *J. Phys. Chem. B* 103:8410–26
44. Purcell EM, Pennypacker CR. 1973. Scattering and absorption of light by nonspherical dielectric grains. *Astrophys. J.* 186:705–14
45. Draine BT, Flatau PJ. 1994. Discrete-dipole approximation for scattering calculations. *J. Opt. Soc. Am. A* 11:1491–99
46. Taflove A. 1995. *Computational Electrodynamics: The Finite-Difference Time Domain Method*. Boston: Artech House
47. McCreery RL. 2000. *Raman Spectroscopy for Chemical Analysis*. New York: Wiley Intersci. 420 pp.
48. Kerker M, Wang DS, Chew H. 1980. Surface enhanced Raman-scattering (SERS) by molecules adsorbed at spherical particles. *Appl. Opt.* 19:4159–74

49. Wang DS, Kerker M. 1981. Enhanced Raman scattering by molecules adsorbed at the surface of colloidal spheroids. *Phys. Rev. B* 24:1777–90
50. Van Duyne RP. 1979. Laser excitation of Raman scattering from adsorbed molecules on electrode surfaces. *Chem. Biochem. Appl. Lasers* 4:101–85
51. Dick LA, Haes AJ, Van Duyne RP. 2000. Distance and orientation dependence of heterogeneous electron transfer: a surface-enhanced resonance Raman scattering study of cytochrome *c* bound to carboxylic acid terminated alkanethiols adsorbed on silver electrodes. *J. Phys. Chem. B* 104:11752–62
52. Whitney AV, Elam JW, Zou SL, Zinovev AV, Stair PC, et al. 2005. Localized surface plasmon resonance nanosensor: a high-resolution distance-dependence study using atomic layer deposition. *J. Phys. Chem. B* 109:20522–28
53. Blatchford CG, Campbell JR, Creighton JA. 1982. Plasma resonance enhanced Raman scattering by adsorbates on gold colloids: the effects of aggregation. *Surf. Sci.* 120:435–55
54. Felidj N, Aubard J, Levi G, Krenn JR, Hohenau A, et al. 2003. Optimized surface-enhanced Raman scattering on gold nanoparticle arrays. *Appl. Phys. Lett.* 82:3095–97
55. Vlckova B, Gu XJ, Moskovits M. 1997. SERS excitation profiles of phthalazine adsorbed on single colloidal silver aggregates as a function of cluster size. *J. Phys. Chem. B* 101:1588–93
56. Doron-Mor I, Barkay Z, Filip-Granit N, Vaskevich A, Rubinstein I. 2004. Ultrathin gold island films on silanized glass: morphology and optical properties. *Chem. Mater.* 16:3476–83
57. Pieczonka NPW, Aroca RF. 2005. Inherent complexities of trace detection by surface-enhanced Raman scattering. *Chemphyschem* 6:2473–84
58. Haynes CL, Van Duyne RP. 2001. Nanosphere lithography: a versatile nanofabrication tool for studies of size-dependent nanoparticle optics. *J. Phys. Chem. B* 105:5599–611
59. Hicks EM, Zhang XY, Zou SL, Lyandres O, Spears KG, et al. 2005. Plasmonic properties of film over nanowell surfaces fabricated by nanosphere lithography. *J. Phys. Chem. B* 109:22351–58
60. Baker GA, Moore DS. 2005. Progress in plasmonic engineering of surface-enhanced Raman-scattering substrates toward ultra-trace analysis. *Anal. Bioanal. Chem.* 382:1751–70
61. Aroca RF, Alvarez-Puebla RA, Pieczonka N, Sanchez-Cortez S, Garcia-Ramos JV. 2005. Surface-enhanced Raman scattering on colloidal nanostructures. *Adv. Colloid Interface Sci.* 116:45–61
62. Kneipp K, Kneipp H, Kneipp J. 2006. Surface-enhanced Raman scattering in local optical fields of silver and gold nanoaggregates: from single-molecule Raman spectroscopy to ultrasensitive probing in live cells. *Acc. Chem. Res.* 39:443–50
63. He L, Musick MD, Nicewarner SR, Salinas FG, Benkovic SJ, et al. 2000. Colloidal Au-enhanced surface plasmon resonance for ultrasensitive detection of DNA hybridization. *J. Am. Chem. Soc.* 122:9071–77
64. Felidj N, Truong SL, Aubard J, Levi G, Krenn JR, et al. 2004. Gold particle interaction in regular arrays probed by surface enhanced Raman scattering. *J. Chem. Phys.* 120:7141–46

65. Gunnarsson L, Bjerneld EJ, Xu H, Petronis S, Kasemo B, Kall M. 2001. Interparticle coupling effects in nanofabricated substrates for surface-enhanced Raman scattering. *Appl. Phys. Lett.* 78:802–4
66. Haes AJ, Haynes CL, McFarland AD, Schatz GC, Van Duyne RR, Zou SL. 2005. Plasmonic materials for surface-enhanced sensing and spectroscopy. *MRS Bull.* 30:368–75
67. Von Raben KU, Chang RK, Laube BL, Barber PW. 1984. Wavelength dependence of surface-enhanced Raman scattering from Ag colloids with adsorbed CN^- complexes, SO_3^{2-}, and pyridine. *J. Phys. Chem. B* 88:5290–96
68. Fornasiero D, Grieser F. 1987. Analysis of the visible absorption and SERS excitation spectra of silver sols. *J. Chem. Phys.* 87:3213–17
69. Carron K, Peitersen L, Lewis M. 1992. Octadecylthiol-modified surface-enhanced Raman spectroscopy substrates: a new method for the detection of aromatic compounds. *Environ. Sci. Technol.* 26:1950–54
70. Ishida T, Hara M, Kojima I, Tsuneda S, Nishida N, et al. 1998. High resolution X-ray photoelectron spectroscopy measurements of octadecanethiol self-assembled monolayers on Au(111). *Langmuir* 14:2092–96
71. Zhang ZS, Wilson OM, Efremov MY, Olson EA, Bruan PV, et al. 2004. Heat capacity measurements of two-dimensional self-assembled hexadecanethiol monolayers on polycrystalline gold. *Appl. Phys. Lett.* 84:5198–200
72. Lewis M, Tarlov M, Carron K. 1995. Study of the photooxidation process of self-assembled alkanethiol monolayers. *J. Am. Chem. Soc.* 117:9574–75
73. Schoenfisch MH, Pemberton JE. 1998. Air stability of alkanethiol self-assembled monolayers on silver and gold surfaces. *J. Am. Chem. Soc.* 120:4502–13
74. Zhang Y, Terrill RH, Tanzer TA, Bohn PW. 1998. Ozonolysis is the primary cause of UV photooxidation of alkanethiolate monolayers at low irradiance. *J. Am. Chem. Soc.* 120:2654–55
75. Love JC, Estroff LA, Kriebel JK, Nuzzo RG, Whitesides GM. 2005. Self-assembled monolayers of thiolates on metals as a form of nanotechnology. *Chem. Rev.* 105:1103–69
76. King F. 1987. *Aluminum and Its Alloys*. New York: Ellis Harwood. 313 pp.
77. Zhang X, Zhao J, Whitney A, Elam J, Van Duyne RP. 2006. Ultrastable substrates for surface-enhanced Raman spectroscopy fabricated by atomic layer deposition: improved anthrax biomarker detection. *J. Am. Chem. Soc.* 128:10304–9
78. Stuart DA, Yuen JM, Shah NC, Lyandres O, Yonzon CR, et al. 2006. In vivo glucose measurement by surface-enhanced Raman spectroscopy. *Anal. Chem.* 78:7211–15
79. Shah NC, Lyandres O, Walsh JT, Glucksberg MR, Van Duyne RP. 2007. Lactate and sequential lactate-glucose sensing using surface-enhanced Raman spectroscopy. *Anal. Chem.* 79:6927–32
80. Abdelsalam ME, Mahajan S, Bartlett PN, Baumberg JJ, Russell AE. 2007. SERS at structured palladium and platinum surfaces. *J. Am. Chem. Soc.* 129:7399–406
81. Mrozek MF, Xie Y, Weaver MJ. 2001. Surface-enhanced Raman scattering on uniform platinum-group overlayers: preparation by redox replacement of underpotential-deposited metals on gold. *Anal. Chem.* 73:5953–60

82. Tian ZQ, Yang ZL, Ren B, Li JF, Zhang Y, et al. 2006. Surface-enhanced Raman scattering from transition metals with special surface morphology and nanoparticle shape. *Faraday Discuss.* 132:159–70
83. Park S, Yang PX, Corredor P, Weaver MJ. 2002. Transition metal–coated nanoparticle films: vibrational characterization with surface-enhanced Raman scattering. *J. Am. Chem. Soc.* 124:2428–29
84. Litorja M, Haynes CL, Haes AJ, Jensen TR, Van Duyne RP. 2001. Surface-enhanced Raman scattering detected temperature programmed desorption: optical properties, nanostructure, and stability of silver film over SiO_2 nanosphere surfaces. *J. Phys. Chem. B* 105:6907–15
85. Hulteen JC, Young MA, Van Duyne RP. 2006. Surface-enhanced hyper-Raman scattering (SEHRS) on Ag film over nanosphere (FON) electrodes: surface symmetry of centrosymmetric adsorbates. *Langmuir* 22:10354–64
86. Cotton TM, Schultz SG, Van Duyne RP. 1980. Surface-enhanced resonance Raman-scattering from cytochrome *c* and myoglobin adsorbed on a silver electrode. *J. Am. Chem. Soc.* 102:7960–62
87. Copeland RA, Fodor SPA, Spiro TG. 1984. Surface-enhanced Raman spectra of an active flavo enzyme: glucose oxidase and riboflavin binding protein on silver particles. *J. Am. Chem. Soc.* 106:3872–74
88. Kneipp K, Moskovits M, Kneipp H, eds. 2006. *Surface-Enhanced Raman Scattering: Physics and Applications*. Berlin: Springer

Annual Review of Analytical Chemistry

Volume 1, 2008

Contents